LTNE approach and simulation for anode-supported SOFCs

Andersson, Martin; Yuan, Jinliang; Sundén, Bengt; Wang, Wei Guo

Published in:
[Host publication title missing]

2009

Appendix to Dissertation: *Solid Oxide Fuel Cell Modeling at the Cell Scale - Focusing on Species, Heat, Charge and Momentum Transport as well as the Reaction Kinetics and Effects* by Martin Andersson, Department of Energy Science, Lund University, 2011, ISBN 978-91-7473-180-4.

Paper II

This paper has been published in:

Proceedings of the 7th International Fuel Cell Science, Engineering & Technology Conference, Newport Beach, California, USA, 2009,
ASME FuelCell2009-85054.

Proceedings of FuelCell2009
ASME 2009 Seventh International Fuel Cell Science, Engineering and Technology Conference
June 8-10, 2009 Newport Beach, California, USA

FuelCell2009-85054

LTNE APPROACH AND SIMULATION FOR ANODE-SUPPORTED SOFCS

Martin Andersson **Jinliang Yuan** **Bengt Sundén**
Department of Energy Sciences, Faculty of Engineering,
Lund University, Box 118, 221 00 Lund, Sweden

Wei Guo Wang
Ningbo Institute of Materials Technology and Engineering (NIMTE),
Chinese Academy of Science (CAS), 315040 Ningbo, People's Republic of China

ABSTRACT
Fuel cells are promising for future energy systems, since they are energy efficient and, when hydrogen is used as fuel, there are no emissions of greenhouse gases. Fuel cells have during recent years various improvements, however the technology is still in the early phases of development, this can be noted by the lack of dominant design both for singe fuel cells, stacks and for entire fuel cell systems. In this study a CFD approach (COMSOL Multiphysics) is employed to investigate the effect on temperature distribution from inlet temperature, oxygen surplus, ionic conductivity and current density for an anode-supported intermediate temperature solid oxide fuel cell (IT-SOFC). The developed model is based on the governing equations of heat-, mass- and momentum transport. A local temperature non equilibrium (LTNE) approach is introduced to calculate the temperature distribution in the gas- and solid phase separately.

The results show that the temperature increasing along the flow direction is controlled by the degree of surplus air. It is also found that the ohmic polarization in the electrolyte and the activation polarization in the anode and cathode have major influence on the performance. If a count flow approach is employed the inlet temperature for the fuel stream should be close to the outlet temperature for the air flow to avoid a too high temperature gradient.

Keywords: SOFC, anode-supported, CFD, COMSOL Multiphysics, LTNE

INTRODUCTION AND PROBLEM STATEMENT
Fuel cells produce electricity and heat directly from chemical conversion of fuel and oxidant energies by electrochemical reactions [1-2]. The fuel cell is not a new invention, because the electrochemical process was discovered already in 1839. However the first real fuel cell system was not designed and built until the 1950s. The interest in fuel cells have been growing exponentially, concerning amount of scientific papers, after year 2000 [3]. Among the various types of fuel cells (FCs), the solid oxide fuel cell (SOFC) has attained significant interest due to its high efficiency and low emissions of pollutants to the environment. High temperature operation offers many advantages, such as high electrochemical reaction rate, flexibility of using various fuels and tolerance to impurities. SOFCs have in general either planar or tubular configurations [1-2, 4]. Fuel cell performance depends on thermal, electro-chemical, mechanical and chemical phenomena [5].

In an electrode supported SOFC either the anode or cathode is relatively thick and works as support material. This design makes it possible to have a very thin electrolyte, i.e. the ohmic losses decreases and the temperature can be lowered to 600-800 °C. Fuel cells working in this temperature range are classified as intermediate temperature (IT) [1, 2] if compared to conventional SOFCs that operate between 800 and 1000 °C [6]. A planar SOFC contains a dense ceramic electrolyte sandwiched between two porous electrodes. The electrolyte contains yttria-stabilized zirconia (YSZ), the cathode strontium doped lanthanium manganite (LSM) and the anode nickel/YSZ [1].

Low temperature (LT)-SOFCs in the range of 300-600 °C is under development, the challenge is to increase the ionic conductivity in the electrolyte. Low temperatures make it possible to use cheaper materials throughout the fuel cell system, i.e., promotion of commercialization. An approach with material development in the nanoscale is expected to be very promising [7].

Fuel cell systems are still an immature technology in early phases of development, as can be noted due to lack of a dominant design, few commercial systems and a low market demand. The creation of strategic niche markets and search for early market niches are of a vital importance for the further development. It is expected that mass production will start when a dominant design is found and production cost will significantly decrease due to economy of scale [3].

Due to complex processes involved in fuel cells, it is not possible to solve the equations describing the physical phenomena analytically, a numerical approach, e.g. the Finite Element Method, needs to be applied to solve the equations in an approximate way [8].

A model that describes physical (mass- heat- and momentum) phenomena inside an anode-supported SOFC is developed, to deeply understand the effect of design and operating parameters. A two-dimensional numerical calculation procedure (CFD approach) is further applied. This study focuses on the effect of ionic electronic conductivity, inlet temperature, surplus of oxygen, current density and count flow. The considered cell includes interconnect, air- and fuel-channels, anode, cathode and electrolyte. Temperature dependent thermal-physical properties are taken into account as well. The temperature distribution in the solid phase and gas phase are calculated separately, based on the LTNE approach.

MATHEMATICAL MODEL

A two-dimensional model for an anode-supported SOFC is developed and implemented in the commercial software COMSOL Multiphysics (version 3.5). Equations for momentum, mass and heat transport are solved simultaneously. The geometry is defined in table 1 and a sketch of the modeled cell can be seen in figure 1. Note the difference in scale between the cell length (x-direction, as in fig. 1) and various thicknesses (y- direction, as in fig. 1). It should be noted that the model in this study is 2D only, and the connection between the electrodes and interconnect can not be explicitly observed in this case.

Oxygen is reduced in the cathode (eqn. 1), and oxygen ions migrate through the electrolyte and reacts then with hydrogen in the anode (eqn. 2) [2, 9].

$$1/2\,O_2 + 2e^- \rightarrow O^{2-} \qquad (1)$$

$$O^{2-} + H_2 \rightarrow H_2O + 2e^- \qquad (2)$$

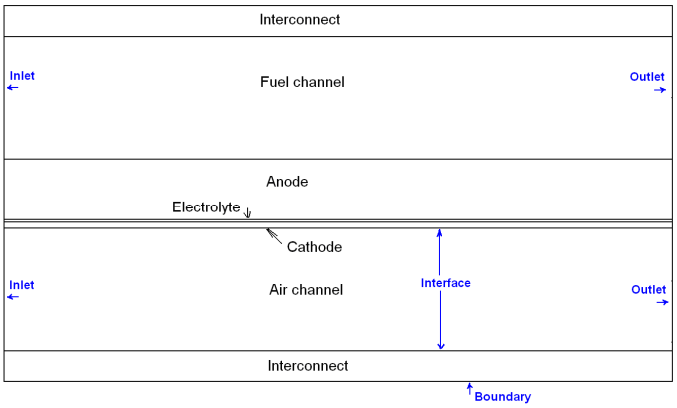

Figure 1: Sketch of an anode-supported SOFC.

Table 1. Cell geometry [6].

Cell length	0.4 m
Fuel channel height	1 mm
Air channel height	1 mm
Anode thickness	500 µm
Cathode thickness	50 µm
Electrolyte thickness	20 µm
Interconnect thickness	500 µm

Governing equations

Momentum equation

The gases flow inside the fuel cell components, such as air- and fuel-channels and porous electrodes. A traditional modeling approach for such a system consists of solving the Darcy's equation in the porous medium and the Navier-Stokes equations in the channels separately. The problem with such an approach is to define interface conditions at the interface between the two domains. It is hard to define this tangential velocity component. To avoid this problem the Darcy-Brinkman equation is introduced and solved for the gas flow in the fuel- and air channels and in the porous media (electrodes) [10, 11].

The Darcy-Brinkman equation (eq. 3) is transformed into the standard Navier-Stokes equation when ($\kappa \rightarrow \infty$) and ($\varepsilon_p = 1$), and into the Darcy equation as $(Da \rightarrow 0)$, Da is the Darcy number. The derivation of Navier-Stokes equation and Darcy equation from Darcy-Brinkman equation can be found in [10].

$$\left(\frac{\nu}{\kappa} + \rho \cdot \nabla \mathrm{u}\right)\mathrm{u} - \nabla\left[-p + \frac{1}{\varepsilon_p}\{\mathbf{T} - (\lambda - \kappa_{dv})(\nabla \mathrm{u})\}\right] = \mathbf{F} \qquad (3)$$

where **F** is the volume force vector, κ is the permeability of the porous medium, ε_p the porosity, v the dynamic viscosity, u the velocity vector and **T** the viscous stress tensor $\left(\mathbf{T} = v\left(\nabla \mathrm{u} + (\nabla \mathrm{u})^T\right)\right)$. κ_{dv} (deviation from thermodynamic equilibrium) is by default set to zero, which means that the fluid particles are in equilibrium with their surrounding. λ is the second viscosity and is, for gases, normally assumed as: λ=-2/3v [12]. The equation for the continuity in the air- and fuel channels reads: $\nabla \mathrm{u} = 0$ [11]. The densities for the participating gases are calculated as [11]:

$$\rho_{mixture} = \frac{p \cdot \sum w_i M_i}{\mathrm{R}T} \tag{4}$$

The dynamic viscosity for each participating spices in the gas phase is calculated as [13]:

$$v_i = \sum_{k=1}^{7} \mathrm{b_k} \cdot \left(\frac{T}{1000}\right)^k \tag{5}$$

where $\mathrm{b_k}$ is the spices dependent parameter and "k" stands for the amount of spices dependent parameters in the viscosity equation. The dynamic viscosity for the gas mixtures is calculated as [13]:

$$v_{mixture} = \sum w_i v_i \tag{6}$$

Mass transport equation

Maxwell-Stefan equation for mass diffusion and convection is used to describe the mass transport phenomena for the gases inside the fuel cell [11]. The Maxwell-Stefan equation is a simplified equation compared to "Dusty Gas Model", since the Knudsen diffusion (collisions between gas molecules and the porous material) is neglected. The reason for this treatment is to reduce the calculation cost and this model is already predefined in COMSOL Multiphysics. However adding the Knudsen diffusion term may increase the diffusion resistance. Maxwell-Stefan equation is solved for the fuel- and air channels and electrodes.

$$\nabla\left(-\rho w_i \sum D_{ij} \nabla x_j + \left(x_j - w_j\right)\frac{\nabla p}{p}\mathrm{u} - D_i^T \frac{\nabla T}{T}\right) + \rho \mathrm{u} \nabla w_j = R_i \tag{7}$$

$$x_j = \frac{w_j}{M_j} M \tag{8}$$

$$\sum_{i=1}^{n} w_i = 1 \tag{9}$$

where w is the mass fraction, x the mole fraction, n the number of species, D_i^T the thermal diffusion coefficient and D_{ij} the Maxwell-Stefan binary diffusion coefficient, R_i the reaction rate, zero in this case since the electrochemical reactions is assumed to take place, and defined, at the interfaces between the electrolyte and electrodes. The electrochemical reactions occur in reality at an active reaction surface area, the tree phase boundary, where gas, ionic and electronic phases meet. The active reaction surface area will be considered in future research when the electrochemical reactions are defined as a source term in the mass transport governing equation instead of an interface condition, as done in this study. The diffusion coefficient in the porous electrodes is calculated as [14, 15]:

$$D_{ij,por} = D_{ij} \cdot \varepsilon_p / t \tag{10}$$

where t is the tortuosity. D_{ij} is calculated as [16]:

$$D_{ij} = \frac{2.66 \cdot 10^{-8} \cdot T^{3/2}}{p \cdot M_{ij}^{1/2} \cdot l_{ij}^2 \Omega_D} \tag{11}$$

$$\Omega_D = \frac{A}{\left(\frac{\mathrm{k'} \cdot T}{\mathrm{e_{ij}}}\right)^B} + \frac{C}{\exp\left(D \cdot \frac{\mathrm{k'} \cdot T}{\mathrm{e_{ij}}}\right)} + \frac{E}{\exp\left(F \cdot \frac{\mathrm{k'} \cdot T}{\mathrm{e_{ij}}}\right)} + \frac{G}{\exp\left(H \cdot \frac{\mathrm{k'} \cdot T}{\mathrm{e_{ij}}}\right)} \tag{12}$$

$$M_{ij} = \frac{2}{\frac{1}{M_i} + \frac{1}{M_j}} \tag{13}$$

$$l_{ij} = \frac{l_i + l_j}{2} \tag{14}$$

$$\mathrm{e_{ij}} = \sqrt{\mathrm{e_i} \cdot \mathrm{e_j}} \tag{15}$$

where Ω_D is the diffusion collision integral, $\mathrm{e_{ij}}$ is the average characteristic Lennard-Jones energy, l_{ij} is the average characteristic length, $\mathrm{M_{ij}}$ is the average molecular weight, and k' is the Boltzmann's constant. A, B, C, D, E, F, G and H are constants, as shown in [16].

Heat transfer equation

The temperature distribution is calculated separately for the gas phase (in air- and fuel-channels and electrodes) and for the solid phase (interconnect, electrodes and electrolyte). Heat is transferred between the phases at the channel walls and in the porous electrodes. The general heat conduction equation is used to calculate the temperature distribution for the solid materials, i.e., electrolyte, interconnect and electrodes [11]:

$$\nabla\left(-k_s \nabla T_s\right) = Q_s \tag{16}$$

where k_s is the thermal conductivity of the solids, T_s the temperature in the solid phase and Q_s are the heat source (heat transfer between the solid- and gas-phase and heat generation due to ohmic polarization). Note that heat generated due to ohmic polarization is assumed to enter the solid phase (as a part of Q_s), heat generation due to electrochemical reactions, concentration- and activation polarization are simplified and defined as interface conditions, as for the mass transport the electrochemical reactions occur in reality at an active reaction surface area. The temperature distribution for the gas mixtures in the fuel- and air- channels and in the porous electrodes is calculated as [11]:

$$\nabla\left(-k_g \nabla T_g\right) = Q_g - \rho_g \cdot c_{p,g} \mathrm{u} \nabla T_g \tag{17}$$

where c_p the heat capacity, T_g the temperature in the gas phase and Q_g the heat transfer between the gas- and solid-phase. Because the Reynolds number is very low, the heat transfer coefficient ($h_{s,g,por}$) in the porous electrodes can, be calculated as [17]:

$$h_{s,g,por} = \frac{2 \cdot k_g}{d_p} \tag{18}$$

where d_p is the electrode particle diameter and k_g the gas conductivity. The heat transfer between the gas phase and solid phase depends on the temperature difference and the particle surface area as [18]:

$$Q_g = h_v\left(T_g - T_s\right) = SA \cdot h_{s,g,por}\left(T_g - T_s\right) \tag{19}$$

where h_v is the volume heat transfer coefficient and SA the surface area (760 000 m^2/m^3 for the cathode and 619 000 m^2/m^3 for the anode [19]). The temperature difference between the solid and gas phase has been found to be neglible (the average temperature difference is 0.0032 K for the cathode and $5.7 \cdot 10^{-5}$ K for the anode) for the situation considered in this study. This small temperature difference between the solid and gas phase in the porous electrodes is due to, the big surface area and very small particle diameter that is assumed for this study. As a comparison it can be mention that the temperature difference between the gas and solid phase where investigated in [17] and calculated to the order of 10^{-2} K, considering porous SOFC electrodes. The heat capacity for each gas specie is calculated as [13]:

$$c_{p,i}(T) = \sum_{k=1}^{7} \mathrm{a_k} \cdot \left(\frac{T}{1000}\right)^k \tag{20}$$

where a_k is the species dependent parameter and "k" stands for the number of parameters in the heat capacity equation. The heat capacities for the gas mixtures can then be calculated when the individual species values are known [13]:

$$c_{p,mixture} = \sum w_i c_{p,i} \tag{21}$$

The gas thermal conductivity for each species in the gas phase is calculated as [13]:

$$k_{g,i}(T) = 0.01 \cdot \sum_{k=1}^{7} \mathrm{c_k} \cdot \left(\frac{T}{1000}\right)^k \tag{22}$$

where c_k is the species dependent parameter and "k" stands for the number of parameters in the thermal conductivity equation. The conductivity for the gas mixtures can then be evaluated as [13]:

$$k_{g,mixture} = \sum w_i k_{g,i} \tag{23}$$

Ohmic polarization occurs due to resistance of the flow of ions in the electrolyte and electrical resistance in the electrodes. The electrodes and electrolyte are heated due to this effect [1,20]:

$$Q_{ohm} = \frac{i \cdot \eta_{ohm}}{\tau} \tag{24}$$

$$\eta_{ohm} = R_{ohm} \cdot i \tag{25}$$

$$R_{ohm} = \frac{\tau_a}{\sigma_a} + \frac{\tau_{el}}{\sigma_{el}} + \frac{\tau_c}{\sigma_c} \tag{26}$$

where τ is the component thickness and R_{ohm} the electrolyte area-specific ohmic resistance. The electronic/ionic conductivities (σ), are calculated as [1, 21]:

$$\sigma_a = \frac{4.2 \cdot 10^7}{T} \cdot \exp\left(\frac{-1200}{T}\right) \tag{27}$$

$$\sigma_{el} = 33.4 \cdot 10^3 \cdot \exp\left(\frac{-10300}{T}\right) \tag{28}$$

$$\sigma_c = \frac{9.5 \cdot 10^7}{T} \cdot \exp\left(\frac{-1150}{T}\right) \tag{29}$$

Boundary and interface conditions

Momentum transport

The boundary conditions for the momentum transport equation are defined as a laminar flow profile for the inlet with an average air inflow velocity of 5.2 m/s (for an oxygen surplus factor of 4). The entrance length due to the build up of a fully developed velocity profile can be neglected since the channel

length is 400 times bigger than the height. The outlet is defined as [11]:

$$v\left(\nabla \mathrm{u} + \left(\nabla \mathrm{u}\right)^{T}\right)\cdot \mathrm{n} = 0 \tag{30}$$

$$p = p_0 \tag{31}$$

where p_0 is a defined outlet pressure. The interfaces between the interconnects and gas channels have to be defined since the governing equation for momentum transport are not solved for the interconnects, the interfaces are defined as walls (u=0). Darcy-Brinkman equation makes it possible to define the interface between the air- and fuel-channels and the porous electrodes as continuous. The Darcy-Brinkman equation is not solved for the electrolyte and interface conditions need to be defined. Oxygen is consumed at the interface between the cathode and electrolyte, and the electrochemical reaction rate depends on the current density. As for the mass transport, the electrochemical reactions occur in reality at an active reaction surface area, but are in this paper simplified and assumed to occur at the interface between the electrodes and electrolyte. The gas velocity effect (r), calculated from the total mass flow given by the electrochemical reaction, on the momentum equation can be calculated as [11]:

$$r = -\frac{i \cdot M_{O_2}}{n_{e,c} \cdot \mathrm{F} \cdot \rho} \tag{32}$$

where i is the current density and $n_{e,c}$ the number of electrons transfer per molecule of oxygen consumed (= 4). At the anode and electrolyte interface one molecule of water is produced for every molecule of hydrogen consumed, and the reaction effect is specified as [11]:

$$r = \frac{i \cdot \left(M_{H_2O} - M_{H_2}\right)}{n_{e,a} \cdot \mathrm{F} \cdot \rho} \tag{33}$$

where $n_{e,a}$ the number of electrons transfer per molecule of hydrogen consumed/water produced (= 2). The implementation of eq. 32 and 33 means that the cell overall mass balances show a very good result.

Mass transport

The boundary conditions for the mass transport equation are defined as mass fraction for the gas channel inlet (w_i=$w_{i,0}$) and the boundaries. However the result can be presented as either mass or mole fraction. The convective flux for the gas channel outlet is defined as [11]:

$$\mathrm{n} \cdot \left(-\rho w_i \sum D_{ij} \left(\nabla x_j + \left(x_j - w_j\right)\frac{\nabla p}{p} \right) - D^T \frac{\nabla T}{T} \right) = 0 \tag{34}$$

The flows from the anode and the cathode to the electrolyte are defined as "Flux" [11]:

$$-\mathrm{n} \cdot \mathrm{N} = n_0 \tag{35}$$

$$\mathrm{N} = -\rho w_i \sum D_{ij} \left(\nabla x_j + \left(x_j - w_j\right)\frac{\nabla p}{p} \right) + D^T \frac{\nabla T}{T} + \rho w_i \mathrm{u} \tag{36}$$

where n stands for the normal vector to the boundary, and n_0 for the inward mass flux [11]:

$$n_0 = \frac{-i \cdot M_i}{n_e \mathrm{F}} \tag{37}$$

where i is the current density and n_e the number of electrons transferred per reaction, and F the Faraday constant. The interfaces between the interconnects and gas channels have to be defined since the governing equation for mass transport are not solved for the interconnects, they are defined as walls (n·N=0).

Heat transfer

As described previously the temperature in the soild and gas phase is calculated separately, heat flows between the phases in the porous material and at the gas channels walls. The inlet temperature is defined by the operating conditions, for the gas flow channel inlet as (T_g=T_0). The outlet for the gas channels is defined as convective flux [11]:

$$-\mathrm{n} \cdot \left(-k \nabla T_g\right) = 0 \tag{38}$$

The boundaries at the top and bottom of the model are defined as symmetry, since it is assumed that the cell is surrounded by other cells with the same temperature distribution. The heat flux at the interface between the interconnects and gas channels as well as at the interface between the gas channels and electrodes is defined as [11]:

$$-\mathrm{n} \cdot \left(-k_s \nabla T_s\right) = q_s \tag{39}$$

$$q_s = h_{s,g,w} \cdot \left(T_{s,w} - T_{g,w}\right) \tag{40}$$

$$q_g = -q_s \tag{41}$$

where T_s is the temperature in the solid phase, T_g the temperature in the gas phase, q_g is the heat flux from the gas phase, q_s the heat flux to the solid phase and $h_{s,g,w}$ the heat transfer coefficient at the gas channel walls [4, 22]:

$$h_{s,g,w} = \frac{Nu \cdot k_g}{\mathrm{c_d}} \tag{42}$$

where *Nu* is Nusselt number, *k* gas phase conductivity and $\mathrm{c_d}$ the channel diameter. The value for Nusselt number (4.094) comes from [22] based on the fully developed flow for rectangular duct, assuming heat flux at two channel walls located opposite to each other, one between the interconnect and the gas channel and between the electrode and gas channel. Heat generated due to electrochemical reactions and due to polarization losses are, as previously described, defined at the electrodes/electrolyte interfaces:

$$-\mathrm{n} \cdot \left(-k \nabla T\right)_- = q_0 \tag{43}$$

$$q_0 = q_r + q_{losses} = -i \cdot \left(\frac{T \cdot \Delta S_r}{n_e \cdot \mathrm{F}} + \eta_{act,e} + \eta_{conc,e} \right) \tag{44}$$

where q_o is the heat generated at the interface (specified as interface condition), q_r the heat generated inside the cell due to change in enthalpy and q_{losses} the heat generated due to potential losses inside the cell. It is assumed that this heat (q_0) is generated in the gas phase. The amount of heat due to electrochemical reactions can be calculated as [9,23]:

$$q_r = -T \cdot \Delta S_r \cdot \dot{n} = -\Delta S_r \frac{T \cdot i}{n_e \mathrm{F}} \tag{45}$$

$$\dot{n} = \frac{i}{n_e \mathrm{F}} \tag{46}$$

where $\dot{n}$ is the molar flux density [mol/(m^{2}s)] and ΔS_r is entropy change of reaction [-50.2 J/(K mol)], and calculated from data in [24]. The heat generation due to activation and concentration polarization can be calculated as [14, 20]:

$$q_{losses} = -i \cdot \left(\eta_{act,e} + \eta_{conc,e}\right) \tag{47}$$

The concentration polarizations due to concentration differences inside the cell are specified as [1]:

$$\eta_{conc,a} = \frac{\mathrm{R}T}{n_{e,a} \mathrm{F}} \ln\left(\frac{p_{H_2O,TPB} \cdot p_{H_2,b}}{p_{H_2,TPB} \cdot p_{H_2O,b}} \right) \tag{48}$$

$$\eta_{conc,c} = \frac{\mathrm{R}T}{n_{e,c} \mathrm{F}} \ln\left(\frac{p_{O_2,b}}{p_{O_2,TPB}} \right) \tag{49}$$

where $p_{i,TPB}$ stands for the partial pressure at three phase boundary (TPB) and $p_{i,b}$ the partial pressure at the interface between gas channel and electrode. Chemical reactions involve energy barriers (i.e., activation polarization) which must be overcome by the reacting species. The activation polarization can be considered as the extra potential needed to overcome the energy barrier of the rate-determining step to a value that the reaction proceeds at a desired rate. It is normally expressed by the Bultler-Volmer equation [14]:

$$i = i_0 \left\{ \exp\left(\beta \frac{n_e \mathrm{F} \eta_{act,e}}{\mathrm{R}T} \right) - \exp\left(-(1-\beta) \frac{n_e \mathrm{F} \eta_{act,e}}{\mathrm{R}T} \right) \right\} \tag{50}$$

where β is the transfer coefficient, and usually assumed to be 0.5. The Bultler-Volmer equation can then be expressed as [1, 14]:

$$i = 2 \cdot i_0 \cdot \sinh\left(\beta \frac{n_e \mathrm{F} \eta_{act,e}}{2\mathrm{R}T} \right) \tag{51}$$

$$\eta_{act,e} = \frac{2\mathrm{R}T}{n_e \mathrm{F}} \sinh^{-1}\left(\frac{i_e}{2 \cdot i_{0,e}} \right) \tag{52}$$

$$i_0 = \frac{RT}{n_e F} k''_e \cdot \exp\left(\frac{-E_e}{\mathrm{R}T} \right) \tag{53}$$

where i_o is the exchange current density. The pre-exponential factor (k'') is $2.35 \cdot 10^{11}$ $\Omega^{-1}\mathrm{m}^{-2}$ for the cathode and $6.54 \cdot 10^{11}$ $\Omega^{-1}\mathrm{m}^{-2}$ for the anode respectively. The activation energy (E) is 137 kJ/mol for the cathode and 140 kJ/mol for the anode [1, 6].

NUMERICAL METHODS

All the governing equations were numerically solved in COMSOL Multiphysics (version 3.5) using a stationary solver with a direct (UMFPACK) linear solver system. The residual convergence was limited to 10^{-6} for all variables. The grid independence was archived at 30 000 finite elements (figure 2), after which the change in maximum temperature was less than 0.1%, change in maximum velocity was less than 1%, oxygen consumption was less than 0.1% and the hydrogen consumption was less than 1% (compared with 53 000 finite elements).

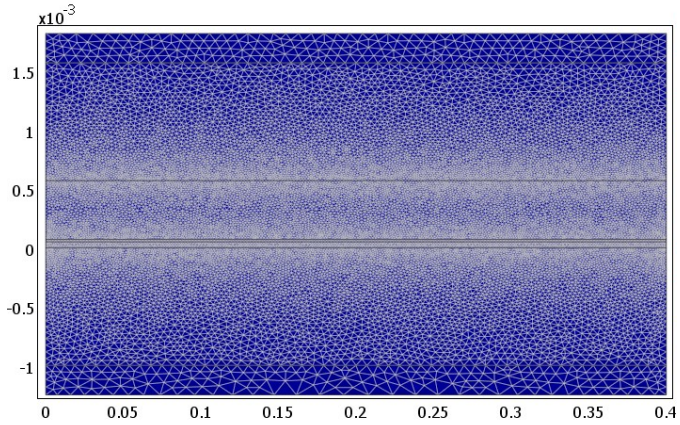

Figure 2: Meshing of the considered geometry.

RESULTS AND DISCUSSION

Material characteristic data typical in literature are used in this study, as shown in table 2.

Table 2. Material characteristic data

$k_{s,a}$	11 W/m/K	[25]
$k_{s,c}$	6 W/m/K	[25]
$k_{s,el}$	2.7 W/m/K	[25]
$k_{s,int}$	20 W/m/K	[25]
$c_{p,a}$	450 J/kg/K	[26]
$c_{p,c}$	430 J/kg/K	[26]
$c_{p,el}$	470 J/kg/K	[26]
$c_{p,int}$	550 J/kg/K	[26]
ρ_a	3310 kg/m^3	[26]
ρ_c	3030 kg/m^3	[26]
ρ_{el}	5160 kg/m^3	[26]
ρ_{int}	3030 kg/m^3	[26]
κ_e	$1.76 \cdot 10^{11}$ m^2	[25]
ε_e	0.5	[25]
d_p	1μm	[15]
t	5	[15]

A base condition is assumed that the cell average current density is 0.3 A/cm^2, surplus factor of oxygen is $S_{O2} = 4$, inlet temperature is 1000 K for both the air- and fuel-channels and the fuel consumption is $C_{fuel} = 80$ mole-%, and flow direction is left -> right. The above parameters are then varied one by one for parameter studies. The surplus of oxygen is specified as:

$$S_{O_2} = \frac{x_{O_2,0}}{x_{O_2,0} - x_{O_2,end}} - 1 \qquad (54)$$

where x_{O2} is the molar fraction of oxygen. The consumption of fuel is specified as:

$$C_{fuel} = \frac{x_{H_2,0} - x_{H_2,end}}{x_{H_2,0}} \qquad (55)$$

The temperature increases along the x-direction (the main flow direction), as seen in fig. 3. The temperature difference in the y-direction inside the air channel occurs because the convective heat flux are bigger in the air channel (compared to the fuel channel) due to the relatively larger gas flow.

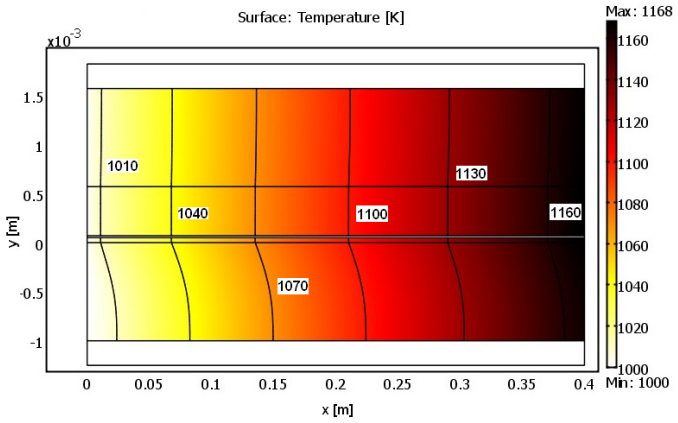

Figure 3: Temperature for the gas phase.

The mole fraction of oxygen (fig. 4) decreases along the flow direction in the air channel and the cathode. There is concentration difference in the y-direction as well, that drives the flow towards the cathode/electrolyte interface, however it is hard to see in the air channel as the cell length is 400 times bigger than the air channel height.

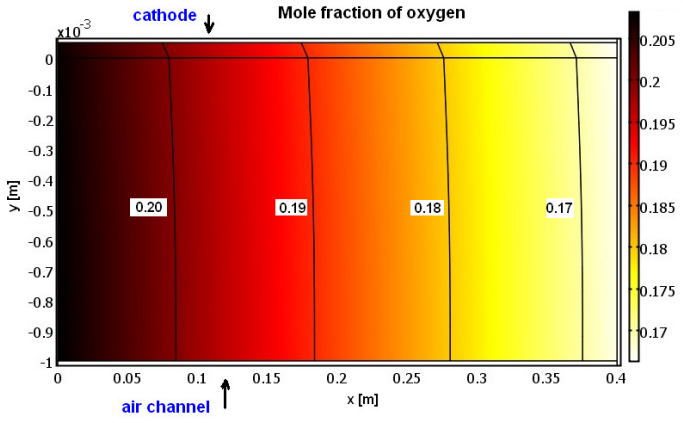

Figure 4: Mole fraction of oxygen in the air channel and cathode

The mole fraction of hydrogen decreases along the flow direction in the fuel channel, as shown in fig. 5. As for the mole fractions in the air channel, there is a concentration difference in the y-direction for hydrogen, which drives the

hydrogen molecules towards the anode/electrolyte interface, however this effect is very small (and impossible to see in the fuel channel), due to the fact that the cell length are is 400 times bigger than the fuel channel height.

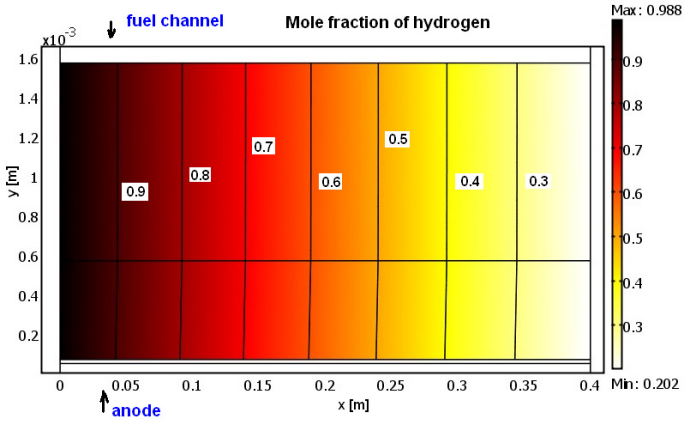

Figure 5: Mole fraction of hydrogen in the fuel channel and anode.

The polarization losses along the flow direction can be seen in fig. 6. It is found that the ohmic polarizations in the electrodes as well as the concentration polarizations are neglible compared to the activation polarizations and the ohmic polarization in the electrolyte, however a small effect from concentration polarization is seen in the anode close to the inlet. This effect is not expected as the highest fuel concentration can be found at the inlet, however the effect on the overall heat balance is found to be neglible. The activation- and ohmic polarizations decrease along the flow direction, as the temperature increase (see fig. 3). It is noted that the activation polarization is more temperature dependent than the ohmic polarization.

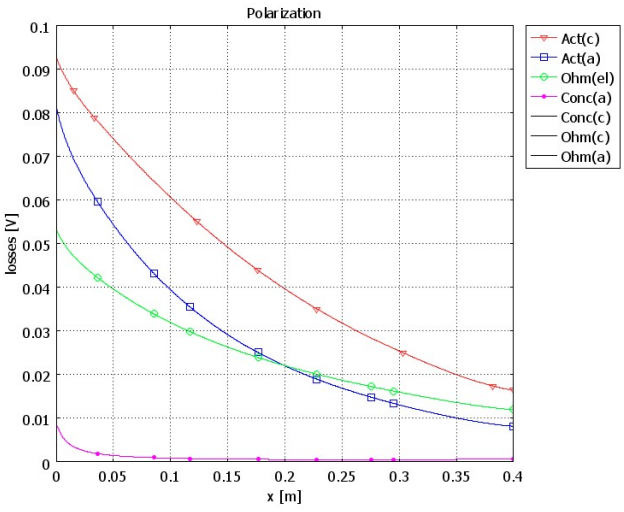

Figure 6: Polarization along the flow direction.

A parameter study is performed to investigate the effect of the oxygen surplus factor, the inlet temperature, the current density, the direction of flow and ionic conductivity. To be able to compare the different investigations with each other, the temperature in the electrolyte is plotted against the position in the flow direction, except for the case with count flow, where the temperatures inside the cell are plotted in two dimensions.

A big surplus flow of oxygen cools down the fuel cell, as can be seen in fig. 7. Change of the oxygen surplus factor is an easy way to control the temperature increase inside the cell, i.e. a higher surplus factor brings a reduced temperature increase along the flow direction. An increased surplus factor also gives a reduced concentration difference in the y-direction, i.e. reduced concentration polarization, however this effect is found to be neglible in this specific study. A higher surplus of oxygen also means that the energy needed in compressors (driving the air flow in the fuel cell system) will increase.

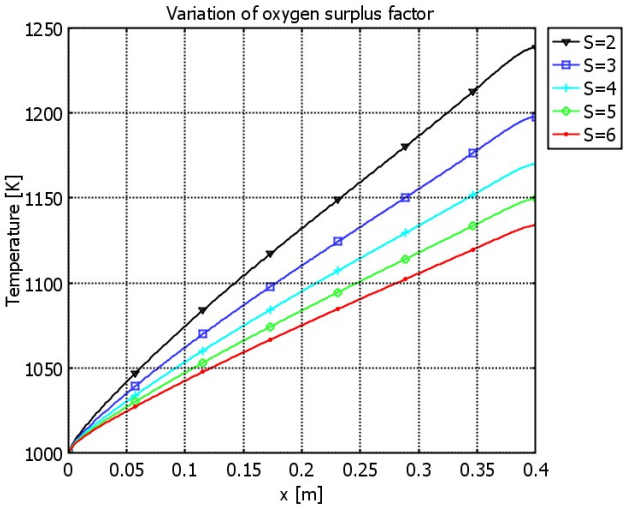

Figure 7: The effect of oxygen surplus factor on temperature along the flow direction in the fuel cell.

An increased inlet temperature gives a reduced temperature increase along the flow direction inside the fuel cell, as can be seen in fig. 8. This is due to the ohmic heating (ohmic polarization) and the activation polarization (inversed temperature dependent). The ohmic heating decreases with increased inlet temperature since the ionic conductivity in the electrolyte increases, also the electronic conductivity in the electrodes increases but this effect is found to be much smaller. Both the ionic conductivity and the exchange current density are material dependent, and it is possible to decrease the polarization losses with development of smart suitable materials.

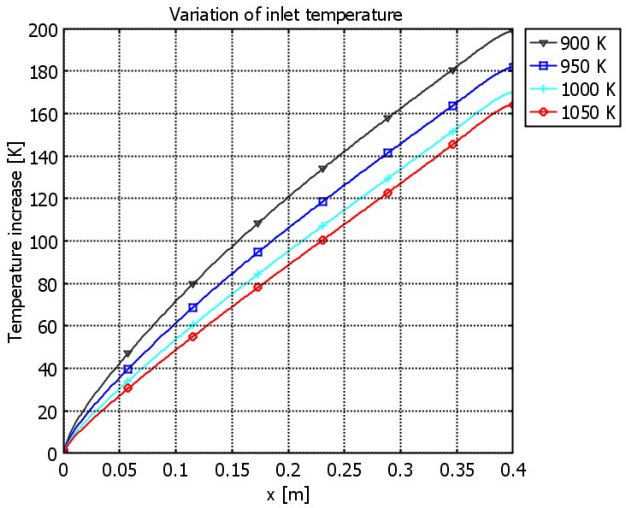

Figure 8: The temperature increase along the flow direction for different inlet temperatures.

The current density influence on the temperature distribution along the flow direction is shown in fig. 9. An increased current density means that the ohmic and activation polarization increase. A higher current density makes it possible to decrease the fuel cell stack size, however extra heat is produced, due to the increased polarization losses.

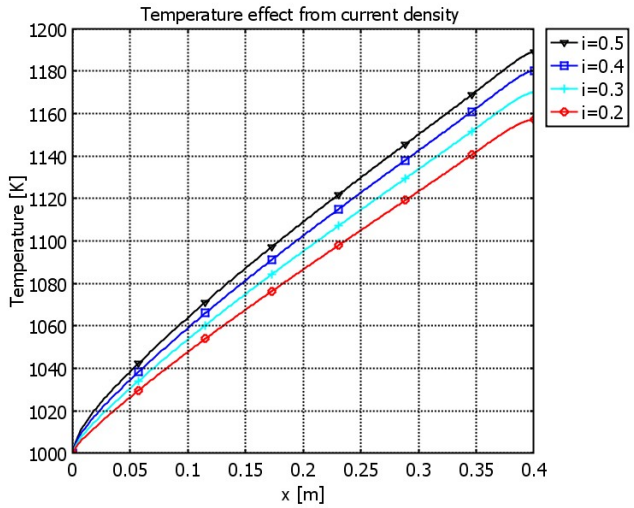

Figure 9: Temperature along the flow direction in the fuel cell for different current densities.

The effect of the ionic conductivity in the electrolyte and the electronic conductivity in the electrodes is investigated. A decreased ionic conductivity in the electrolyte make it harder for the oxygen ions to pass through the electrolyte and the ohmic polarization increases, i.e. the temperature within the cell increases, as seen in fig. 10. "50%" means that the ionic conductivity in the electrolyte is halved, and "200%" means that the ionic conductivity is doubled.

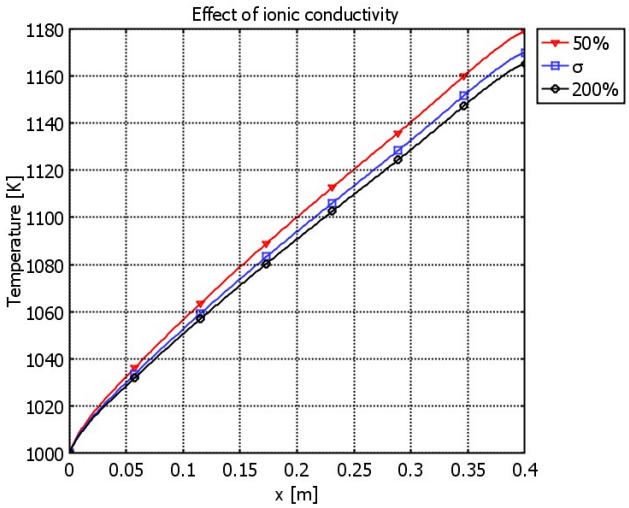

Figure 10: Temperature distribution along the flow direction for different ionic/electronic conductivities.

A simulation is also conducted to study the effect of count flow, i.e. the air enters into the fuel cell on one side (x = 0.4 m) and the fuel from the opposite side (x = 0), see figure 11. Both the air and fuel gas enter the cell at 1000 K. The fuel flow is cooled down by the air flow along the channel and the outlet temperature for the fuel gas stream is found to be close to the inlet temperature of the air flow. As the fuel gas stream enters into the cell it is quickly heated up to a temperature close to the outlet temperature of the air flow, and it is expected that this large temperature gradient will cause material problems. It is recommended for count flow to try to keep the inlet temperature of the fuel stream as close as possible to the outlet temperature of the air stream. Both the temperature gradient inside the cell and the maximum temperature are bigger for a count flow design, compared to the basic case:

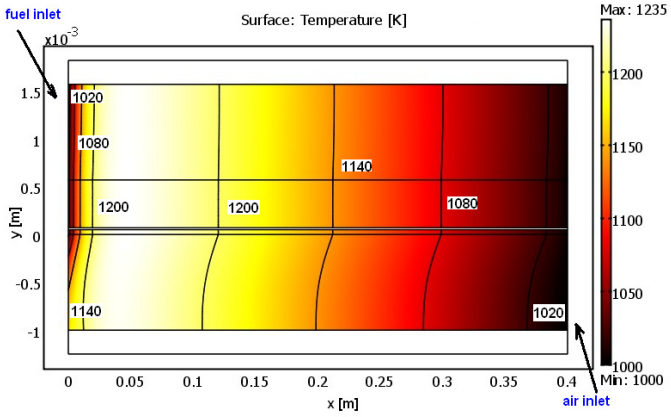

Figure 11: The temperature along the x-axis in count flow

CONCLUSIONS

In this study, a CFD approach is developed and implemented to analyze physical phenomena that take place inside an anode-supported SOFC. Equations for heat-, mass- and momentum transport are solved simultaneously. A LTNE approach is applied to calculate the temperatures in the solid phase and gas phase separately. It is concluded that the temperature difference is neglible for the investigated conditions. It is found that activation polarization for both the anode and cathode as well as ohmic polarization in the electrolyte cause a significant effect on the temperature in intermediate temperature range. An increased inlet temperature decreases the polarization losses within the cell, however an increased operation temperature requires more expensive materials. An optimization should be done considering the current density and stack size (i.e., production cost). The ionic conductivity in the electrolyte can be increased with more advanced material or design. It is found that changing the oxygen surplus factor is an easy approach to control the temperature increase within the cell. It is revealed that it is important for the count flow design to keep the inlet temperature of the fuel stream close to the outlet temperature of the air stream to avoid too high temperature gradients close to the fuel flow inlet.

NOMENCLATURE

$\dot{n}$	molar flux density, mol/(m^{2}s)
C	consumption, dimensionless
c_d	channel diameter, m
c_p	specific heat capacity at constant pressure, J/kg/K
Da	Darcy number, dimensionless
D_{ij}	Maxwell-Stefan binary diffusion coefficient, m^2/s
D_i^T	thermal diffusion coefficient, kg/(m·s)
d_j	diffusional driving force, dimensionless
d_p	electrode particle diameter, m
E	activation energy, kJ/mol
e	characteristic Lennard-Jones energy, K
F	volume force vector, N/m^3
F	Faraday constant, 96485 C/mol
$h_{s,g}$	heat transfer coefficient, W/(m^{2}K)
h_v	volume heat transfer coefficient, W/(m^{3}K)
i	current density, A/cm^2
i_0	exchange current density, A/cm^2
k'	Boltzmann's constant, J/K
k	thermal conductivity, W/m/K
k''	pre-exponential factor, 1/(Ωm^2)
l_{ij}	characteristic length, Å
M	molar mass of the mixture, kg/mol
M_j	molar mass of species j, kg/mol
n_0	inlet mass flux, kg/m^2/s
n_e	number of electrons transferred per reaction
Nu	Nusselt number, dimensionless
p	pressure, Pa
q	heat flux, W/m^2
Q	source term (heat), W/m^3
Q'	source term (mass), kg/(m^{3}s)
r	velocity effect due to electrochemical reaction, m/s
$\bar{r}$	average pore ratio, m
R	gas constant, 8.314 J/mol/K
R_i	reaction rate, kg/m^3/s
R_{ohm}	electrolyte area-specific ohmic resistance, Ω/m^2
S	surplus factor, dimensionless
SA	surface area, m^2/m^3
ΔS_r	entropy of reaction, J/K/mol
T	temperature, K
T	viscous stress tensor, N/m
t	tortuosity, dimensionless
u	velocity field, m/s
v	dynamic viscosity, Pa·s
w_i	mass fraction of species i, kg/kg
x, y	coordinate system, m
x_j	molar fraction of species j, mol/mol

Greek symbols

ε	porosity, dimensionless
η	over potential, V
κ	permeability, m^2
κ_{dv}	deviation from thermodynamic equilibrium, Pa·s
ρ	density, kg/m^3
σ	ionic/electronic conductivity, Ω^{-1}m^{-1}
τ	component thickness, m
Ω_D	diffusion collision integral, dimensionless

Subscripts

0	initial
a	anode
act	activation polarization
c	cathode
conc	concentration polarization
e	electrode, $e \in \{a, c\}$
el	electrolyte
g	gas phase
H_2	hydrogen
H_2O	water
i	molecule i
int	interconnect
j	molecule j
K	Knudsen diffusion
losses	activation and concentration polarization
O_2	oxygen
ohm	ohmic polarization
por	porous media
s	solid phase
TPB	three phase boundary
w	gas channel wall

ACKNOWLEDGMENTS

The Swedish Research Council (VR) and VR-Sida Swedish Research Links support the current research.

REFERENCES

[1] Patcharavorachot Y., Arpornwichanop A., Chuachuebsuk A., Electrochemical study of a planar solid oxide fuel cell: Role of support structures, *J. Power Sources*, **177**, pp. 254-261, 2008

[2] Andersson M., Yuan, J, Sundén B., Chemical Reacting Transport Phenomena and Multiscale Models for SOFCs, Proceedings of *Heat Transfer 2008,* WIT Press, UK, 2008

[3] Saxe M., Bringing fuel cells to reality and reality to fuel cells, Doctoral thesis, KTH- Royal Institute of Technology, 2008

[4] Yuan J., Yang G., Andersson M., Sundén B., CFD approach for chemical reaction coupled heat transfer in SOFC channels, Proceedings of *7th International Symposium on Heat Transfer (ISHT7),* Beijing, China, 2008

[5] Reifsnider K., Huang X., Ju G., Solasi R., Multi-scale Modeling Approaches for Functional Nano-composite Materials, *J. Mater. Sci.*, **41**, pp. 6751-6759, 2006

[6] Aguiar P., Adjiman C.S., Brandon N.P., Anode-supported intermediate temperature direct internal reforming solid oxide fuel cell. I: model-based steady-state performance, *J. Power Sources* **138**, pp.120-136, 2004

[7] Zhu B., Next generation fuel cell R&D, *Int. J. of Energy Res*., **30**, pp. 895-903, 2006

[8] Kemm M., Dynamic solid oxide fuel cell modelling for non-steady state simulation of system applications, Doctoral thesis, Lund University, 2006

[9] Bove R. Ubertini S., Modeling solid oxide fuel cell operation: Approaches, techniques and results, *J. Power Sources*, **159**, pp. 543-559, 2006

[10] Le Bars M., Grae Worster, M., Interfacial conditions between a pure fluid and a porous medium, implications for binary alloy solidification, *J. Fluid Mech.*, **550**, pp.149-173, 2006

[11] COMSOL Multiphysics 3.5 user guide, 2008

[12] Versteeg H.K., Malalasekera W., An introduction to computational fluid dynamics - The finite volume method, Pearson Education Limited, 1995

[13] Todd B., Young J.B., Thermodynamic and transport properties of gases for use in solid oxide fuel cell modeling, *J. Power Sources*, **110**, pp. 186-200, 2002

[14] Chan, S.H., Khor K.A., Xia Z.T., A complete polarization model of a solid oxide fuel cell and its sensitivity to change of cell component thickness, *J. Power Sources*, **93**, pp.130-140, 2001

[15] Nordelöf A., Salsing C., SOFC Modeling in FEMLAB, Chalmers University Sweden, Master thesis, 2003

[16] Reid R.C., Prausnitz J.M., Poling B.E., The properties of gases & liquids, fourth edition, R.R. Donnelley & Sons Company, 1986

[17] Damm D.L., Fedorov A.G., Local thermal non-equlibrium effects in porous electrodes of the hydrogen fueled SOFC, *J. Power Sources*, **159**, pp. 1153-1157, 2006

[18] Chao C.H., Hwang A.J.J., Predictions of phase temperatures in a porous cathode of polymer electrolyte fuel cells using a two-equation model, *J. Power Sources*, **160**, pp. 1122-1130, 2006

[19] Marrero-López D., Ruiz-Morales J.C. Peña-Martínez J., Canales-Vázquez J., Núñez P., Preparation of thin layer material with macroporous microstructure for SOFC applications, *J. Solid State Chemistry*, **181**, pp.685-692, 2008

[20] Chan S.H., Low C.F., Ding O.L., Energy and exergy analysis of simple solid-oxide fuel-cell power systems, *J. Power Sources*, **103**, pp. 188-200, 2002

[21] Ferguson J.R., Fiard J.M. Herbin R., Three dimensional numerical simulation for various geometries of solid oxide fuel cells, *J. Power Sources*, **58**, pp. 109-122, 1996

[22] Shah R.K., London A.L., Laminar flow forced convection in ducts. Academic Press , London, 1978

[23] Janardhanan V.M., Deutschmann O., Numerical study of mass and heat transport in solid-oxide fuel cells running on humidified methane, *Chem. Eng. Sci*., **62**, pp. 5473-5486, 2007

[24] Bessler W.G., Warnatz J., Goodwin D.G., The influence of equilibrium potential on the hydrogen oxidation kinetics of SOFC anodes, *Solid State Ionics*, **177**, pp. 3371-3383, 2007

[25] Kakac S., Pramuanjaroenkij A., Zhou X.Y., A review of numerical modeling of solid oxide fuel cells, *Int. J. Hydrogen Energy*, **32**, pp.761-786, 2006

[26] Janardhanan V.M., Deutschmann O., Numerical study of mass and heat transport in solid-oxide fuel cells running on humidified methane, *Chem. Eng. Sci.*, **62**, p. 5473-5486, 2007